

An infrared measurement of chemical desorption from interstellar ice analogues

Y. Oba^{1*}, T. Tomaru¹, T. Lamberts², A. Kouchi¹ and N. Watanabe¹

¹Institute of Low Temperature Science, Hokkaido University, Sapporo, Hokkaido, Japan.

²Institute for Theoretical Chemistry, University of Stuttgart, Stuttgart, Germany.

*e-mail: oba@lowtem.hokudai.ac.jp

In molecular clouds at temperatures as low as 10 K, all species except hydrogen and helium should be locked in the heterogeneous ice on dust grain surfaces. Nevertheless, astronomical observations have detected over 150 different species in the gas phase in these clouds. The mechanism by which molecules are released from the dust surface below thermal desorption temperatures to be detectable in the gas phase is crucial for understanding the chemical evolution in such cold clouds. Chemical desorption, caused by the excess energy of an exothermic reaction, was first proposed as a key molecular release mechanism almost 50 years ago¹. Chemical desorption can, in principle, take place at any temperature, even below the thermal desorption temperature. Therefore, astrochemical network models commonly include this process^{2,3}. Although there have been a few previous experimental efforts⁴⁻⁶, no infrared measurement of the surface (which has a strong advantage to quantify chemical desorption) has been performed. Here, we report the first infrared in situ measurement of chemical desorption during the reactions $\text{H} + \text{H}_2\text{S} \rightarrow \text{HS} + \text{H}_2$ (reaction 1) and $\text{HS} + \text{H} \rightarrow \text{H}_2\text{S}$ (reaction 2), which are key to interstellar sulphur chemistry^{2,3}. The present study clearly demonstrates that chemical desorption is a more efficient process for releasing H_2S into the gas

phase than was previously believed. The obtained effective cross-section for chemical desorption indicates that the chemical desorption rate exceeds the photodesorption rate in typical interstellar environments.

Astronomically abundant molecules, such as H₂, H₂O and CH₃OH, can be synthesized on icy dust grains by hydrogen addition to H, O and CO, respectively⁷⁻⁹, and some of these molecules are released into the gas phase from low-temperature grains. One of the non-thermal processes often proposed is photodesorption⁷, which has been experimentally demonstrated to play an important role in photon-dominated regions¹⁰⁻¹². However, photodesorption would be inefficient in dense regions where the ultraviolet field is very weak. Therefore, additional desorption processes need to be invoked. The importance of chemical desorption has been recognized mainly in the modelling community to explain the gas phase abundances of molecules that have originated on a surface. Indeed, chemical desorption with varying efficiencies has been incorporated into chemical models^{2,3}. It is certainly the least well understood of the gas-grain processes that govern the results of astrochemical models to a large extent¹³. One might simply assume that most of the reaction products desorb from the surface after a reaction has taken place because, in general, the exothermicity (several eV) is significantly larger than the hydrogen bonding and physisorption energies (<0.5 eV) expected for adsorbates on dust grains. However, surprisingly, infrared in situ measurements for surface hydrogenation reactions; for example, CO hydrogenation to produce H₂CO and CH₃OH, have indicated that most of these products remain on the surface^{14,15}. Previous experiments focusing on quantifying the efficiency of chemical desorption were performed by gas phase detection solely with the use of a quadrupole

mass spectrometer (QMS)⁴⁻⁶. In these experiments, the extent of desorption was derived only from the gas phase measurements. In contrast, infrared measurements can detect species on the substrate. Since chemical desorption is certainly a surface process, to monitor surface species by infrared measurements is crucial for a complete understanding of the chemical desorption phenomenon. In addition, time-resolved infrared measurements are necessary for obtaining chemical desorption cross-sections, which are highly desirable for chemical modelling studies. The present experiment, which takes an ideal reaction system where the reactant and product are both H₂S, enables us to quantify desorption after a reaction by in situ infrared absorption spectroscopy. In our reaction system, reaction 1 (R1) occurs between an H₂S molecule and an H atom. R1 is expected to proceed by quantum tunnelling through a moderate activation barrier of about 1,560 K¹⁶, while H atom addition to form H₃S is unlikely to occur¹⁷. The reactions of HS with H₂ and H₂O are both endothermic and are thus inhibited at low temperatures. As a result, HS on the ice can only react again with an H atom to produce H₂S (reaction 2 (R2)). That is, we can eliminate the ambiguity arising from the uncertainties in the absorption coefficients of different parent and product molecules.

The experimental details are summarized in the Methods. Briefly, solid H₂S is produced on an ice dust analogue, amorphous solid water (ASW), by gaseous H₂S deposition at 10 K. This is subsequently exposed to H atoms, which were produced by the dissociation of H₂ with an efficiency of >60%. Variations in the H₂S abundance are monitored in situ using a Fourier-transform infrared (FTIR) spectrometer in reflection mode. Furthermore, to confirm the FTIR measurements for chemical desorption, following atom exposure, a temperature programmed desorption (TPD) experiment is

performed to measure both the unreacted parent H₂S and the reaction product (R2) that are present on the surface. A ramping rate of 4 K min⁻¹ is used until a final temperature of 200 K is reached.

Figure 1 shows the FTIR spectrum of solid H₂S (0.7 monolayer; 1 monolayer is equivalent to 1×10^{15} molecules cm⁻²) deposited on ASW at 10 K, as well as the difference spectra after exposure to H atoms for up to 120 min. Since the surface area of ASW under our experimental conditions is about ten times larger than that of a flat crystalline surface¹⁵, the H₂S coverage on ASW should correspond to ~0.07. Figure 1 clearly shows a decrease in the peak intensity for the S–H stretching band of solid H₂S (2,570 cm⁻¹)^{18,19} upon H atom exposure. No other sulphur-bearing species, such as H₂S₂ (~2,500 cm⁻¹) or HS₂ (2,483 cm⁻¹)¹⁹ are observed besides H₂S. In addition, disulphur (S₂), which is infrared inactive, was not detected during the TPD experiment. Furthermore, we confirmed that no decrease in H₂S is observed when solid H₂S is exposed only to H₂ molecules on ASW. This indicates that the impact of H₂ on H₂S induces neither a reaction nor desorption. The surface abundance of H₂S gradually decreased, levelling off at 60% of the initial amount of H₂S (Fig. 2), while 40% of the H₂S remained on the surface after 120 min without desorbing. Figure 3 shows TPD spectra of H₂S (m/z = 34) after exposure to H atoms or H₂ molecules for 120 min. Both spectra show three peaks at 95, 145 and 160 K, which are attributable to (1) the desorption of H₂S from the top of the ASW surface, (2) H₂S emitted via a molecular volcano process and (3) co-desorption with H₂O, respectively²⁰. After 120 min, the total TPD peak area for H atom exposure was about 55% of that for H₂ exposure only.

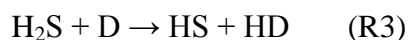
Both the FTIR spectra and TPD measurements thus clearly demonstrate that chemical desorption is induced by reactions with H atoms. From the TPD measurement,

however, the amount of remaining H₂S is 15% larger than that measured by FTIR spectrometry because the TPD measurements detected H₂S desorbed from not only the sample surface exposed to H atoms but also non-exposed areas of the cold head. The remnant undesorbed H₂S may be related to the adsorption sites on the ASW surface, as previously reported^{8,21}. Porous ASW is known to have various adsorption sites with different associated adsorption energies⁸. H₂S molecules adsorbed in the potentially shallow sites may preferentially react with H atoms, leading to desorption. In contrast, the reaction of H atoms with H₂S in the deeper sites may be significantly suppressed, resulting in the presence of unreacted H₂S even after long exposure. This interpretation is supported by the fact that a larger fraction of H₂S (~80%) desorbed from the surface of polycrystalline ice (Supplementary Fig. 1), which has fewer deep sites because of its surface flatness⁸.

It is not a priori clear whether chemical desorption occurs during R1 or R2. The heats of reaction for R1 and R2 are ~0.6 and 3.8 eV, respectively. In principle, both reactions may cause desorption of products or intermediates because heats of reaction are larger than typical energies for physisorption and hydrogen bonding with the ASW surface. For the product of R1, the binding energy of HS to small water clusters is ~0.1 eV (see Methods), which is of the same order as the reaction heat. For R2, the binding energy of the H₂S product to the same water clusters, as mentioned above, is also ~0.1 eV. When comparing differences in the heats of reaction and binding energies of R1 and R2, we deduce that desorption is more likely to be favourable in R2.

So far, we have assumed that both R1 and R2 occur. To confirm this, we performed additional experiments in which solid H₂S was exposed to D atoms instead of H atoms on ASW at 10 K. The formation of deuterated sulphides (HDS and D₂S) was

then expected by successive H–D substitution reactions:



The infrared measurements and subsequent TPD experiments certainly confirm the formation of deuterated species (Fig. 4; see also Supplementary Fig. 2). This observation of HDS and/or D_2S is clear evidence for the occurrence of not only R3–R6, but also R1 and R2. In this measurement, we did not quantify the chemical desorption because of the lack of experimental data for the absorption coefficient of HDS on ASW. In addition, we confirmed that when D_2S was exposed to D atoms on the surface of amorphous solid D_2O at 10 K, about 40% of the initial D_2S was found to desorb after 120 min (Supplementary Fig. 3). The difference in the desorption fractions is not easy to explain simply by the mass difference between H_2S and D_2S and thus might originate in reaction dynamics.

In interstellar clouds, the main sulphur reservoir is commonly proposed to be present in an undetected form on dust grains^{3,22,23}. Grain surface or ice chemistry is known to be of key importance in the interstellar formation of water and methanol and may also lead to more complex species²⁴. H_2S can be an important carrier of sulphur atoms in ice²⁵. Modelling and observational studies also seem to indicate this^{26,27}. So far, to the best of our knowledge, the models for H_2S chemistry in the early stages of star formation either include chemical desorption with ~1% efficiency per reactive event or do not include this at all^{2,3,23}. In the present experiment, we determine an effective chemical desorption cross-section of $2.2 \times 10^{-17} \text{ cm}^2$ by fitting the H_2S attenuation to a

single-exponential curve (Fig. 2; see Methods for the meaning of ‘effective cross-section’). This value is comparable with the ultraviolet absorption cross-section of solid H_2S ²⁸. However, given that the photodesorption cross-section should be lower than the absorption cross-section, the effective chemical desorption cross-section may be larger than the photodesorption cross-section. In addition, assuming that the number density of H atoms is 10 cm^{-3} at a temperature of 10 K in dense clouds, the H atom flux is estimated to be $\sim 10^5\text{ cm}^{-2}\text{ s}^{-1}$, which is about one to two orders of magnitude higher than the ultraviolet photon flux^{29,30}. Under these conditions, the chemical desorption for H_2S is likely to exceed photodesorption. As described above (see also Fig. 2), 40% of the initial deposited H_2S remains on the surface while 60% of this is lost (desorbs) (see Methods for more details and the experimental meaning of ‘efficiency’). When the chemical desorption efficiency, which includes desorption of both H_2S and HS, is defined by the number of chemically desorbed molecules relative to the total number of initial molecules, its value is 60%.

We have successfully determined the effective cross-sections for the chemical desorption of H_2S from ASW by in situ infrared measurements. We wish to stress, however, that the chemical desorption process depends on the specific reaction system at hand and, therefore, it will still be necessary to examine other molecules in the future. To fully understand surface reactions, it is essential in chemistry to know how exothermicity is used for desorption as well as dissipation into the bulk and/or in internal and kinetic motions of the molecule. Therefore, the present report has a significant impact on both astronomy and fundamental chemistry.

Methods

Apparatus. All experiments were performed using an ultra-high vacuum reaction system that was mainly composed of a stainless steel ultra-high vacuum chamber with a reflection-absorption-type FTIR spectrometer and a QMS. A gold-coated substrate was located at the centre of the apparatus, which was connected to a He cryostat. The substrate temperature could be controlled from 5 to 300 K. The base pressure inside the reaction chamber was of the order of 10^{-8} Pa. Gaseous species were deposited through a capillary plate at an angle of 45° to the surface normal.

Experimental. ASW was first produced on the substrate at 10 K by the vapour deposition of gaseous H_2O at a deposition rate of ~ 2 monolayers min^{-1} , where one monolayer corresponds to 1×10^{15} molecules cm^{-2} . The thickness of the ASW was adjusted to 30 monolayers based on the peak area and the band strength of the O–H stretching band of H_2O at $3,300 \text{ cm}^{-1}$ (ref. 31). Gaseous H_2S was then deposited on the ASW at 10 K at a deposition rate of 1 monolayer min^{-1} . The thickness of solid H_2S was adjusted to 0.7 monolayer, which was evaluated based on the peak area and the band strength of the S–H stretching band at $\sim 2,570 \text{ cm}^{-1}$ (ref. 18). The formed H_2S was exposed to H atoms, which were produced by the dissociation of H_2 molecules in a microwave-induced plasma. The dissociation fraction of H_2 in the plasma was more than 60% under these experimental conditions³². The H atoms were cooled to ~ 100 K before leaching to the substrate through multiple collisions with the inner wall of an aluminium pipe, which was cooled to the liquid N_2 temperature. As a blank experiment, solid H_2S was exposed to H_2 molecules only for 120 min to evaluate the effect of the co-deposited H_2 on the desorption of H_2S . This experiment is denoted as a H blank experiment.

An additional experiment was performed on polycrystalline H₂O (c-H₂O) ice, which was prepared by the production of ASW at 10 K with a thickness of 30 monolayers, followed by increasing the substrate temperature to 150 K and subsequently reducing it back to 10 K. Next, 0.7 monolayer H₂S was deposited on the c-H₂O and this was exposed to H atoms for up to 120 min. Solid H₂S (0.7 monolayer) was exposed to D atoms to confirm whether reactions R3–R6 occur on ASW (30 monolayers). D atoms were produced by a similar method to that for H atoms, where D₂ molecules were dissociated in microwave-induced plasma and cooled to 100 K.

Chemical desorption of D₂S was also studied in another experiment. Gaseous D₂S was deposited on pre-deposited deuterated water (D₂O) at 10 K. The abundances of D₂O and D₂S were adjusted to those of H₂O and H₂S in the former experiments based on the peak area of the O–D (2,570 cm⁻¹) and S–D stretching bands (1,860 cm⁻¹) and their band strengths, respectively^{18,33}. The prepared solid sample was exposed to cold D atoms for up to 120 min. As a blank experiment, solid D₂S was exposed to D₂ molecules only, for which we confirmed no desorption of D₂S even after D₂ exposure for 120 min. The fluxes of H and D atoms were estimated as 1.3×10^{14} and 2.6×10^{14} atoms cm⁻² s⁻¹, respectively, according to a procedure described previously³⁴.

After the atom or molecule exposure experiments, we performed a TPD experiment, in which each sample was heated to 200 K at a constant ramping rate of 4 K min⁻¹ and the desorbed species from the substrate were recorded with the QMS.

Efficiency of chemical desorption. There can be several definitions for the chemical desorption efficiency. In previous studies where a QMS was used as a tool for estimating chemical desorption, the chemical desorption efficiencies were generally

derived from the fraction of the target molecule remaining after reactions on the substrate^{4,5,35,36}. For comparison with previous studies, here, we use a similar definition; that is, the number of chemically desorbed molecules relative to the total number of initial molecules at the termination of reactions. Due to some potential difficulties on QMS, the derived chemical desorption efficiencies often have large errors⁵. In contrast, owing to the visibility of the H₂S decrease on the infrared spectrum (Fig. 1), the desorption efficiency in the present study was—regardless of desorbed species—determined to be exactly 60% under the present experimental conditions (Fig. 2). However, it should be noted that the value can change with the fluence of atoms.

There is difficulty when modellers take the value of efficiency from experimental works because the definition of ‘per reactive event’ is generally used in the models while experiments on the surface reaction never provide values per reactive event. Unlike for the gas-phase beam experiment, the single collision condition cannot be controlled in experiments on surface reactions. Instead, we propose the additional chemical desorption efficiency under a different definition: a desorption yield per incident H atoms. In the earlier stages of the reaction (<5 min), the column density of H₂S linearly decreased with H atom exposure time (Fig. 2). During this period, the decrease of H₂S via chemical desorption was $\sim 2.1 \times 10^{14}$ molecules cm⁻². Since the H atom fluence during 5 min is 3.9×10^{16} atoms cm⁻², the chemical desorption yield per incident H atom was calculated to be 5.4×10^{-3} . However, since most of the H atoms land on ASW and should recombine to yield H₂ when the flux of H atoms is very high³⁷, the actual number of H atoms that reacted with H₂S should be much smaller than the calculated H fluence (that is, 3.9×10^{16} atoms cm⁻²). Therefore, the above calculated efficiency should be the lower limit under the present experimental conditions.

Moreover, in realistic interstellar environments where the H atom flux is much lower than under laboratory conditions, each H atom landing on a dust grain has a greater chance of encountering reactants besides other H atoms. As a result, the chemical desorption efficiency defined by per incident H atom should be sufficiently enhanced under realistic conditions. However, note again that the chemical desorption yield per incident H atom is not equivalent to that per reactive event.

Effective cross-section. By simply assuming that the chemical desorption of H₂S proceeds through a single process such as photodesorption, the relative abundance of H₂S can be represented as a single exponential decay curve as follows:

$$\Delta[\text{H}_2\text{S}]_t / [\text{H}_2\text{S}]_0 = A(1 - \exp(-\sigma\phi t)) \quad (1)$$

where $\Delta[\text{H}_2\text{S}]_t$, A , σ and ϕ represent the variation in the abundance of H₂S at time t , a saturation value for the desorption fraction of H₂S, the effective cross-section of chemical desorption in cm² and the flux of H atoms ($\sim 1.3 \times 10^{14}$ atoms cm⁻² s⁻¹), respectively. By fitting the plots in Fig. 2 into equation (1), we obtain $\sigma = 2.2 \times 10^{-17}$ cm² for the chemical desorption of H₂S from ASW, as described in the main text. Likewise, the effective cross-sections for the chemical desorption of H₂S from c-H₂O and D₂S from amorphous solid D₂O were calculated to be 5.3×10^{-18} and 3.5×10^{-18} cm², respectively. This assumption may be optimistic; nevertheless, we believe that the obtained order of magnitude of the effective cross-section is sufficient to conclude that chemical desorption of H₂S would be very effective even in dense clouds where the H atom number density is much lower than that in the experiment, and thus the ratio of the collision frequency between H atoms and H₂S to that between two H atoms, frequency(H-H₂S)/frequency(H-H), is enhanced.

Binding energy of HS and H₂S. To estimate the binding energies of HS and H₂S on a water surface, we optimized two clusters consisting of seven water molecules, both with and without the adsorbates. The binding energy is defined as the energy difference between the gas phase adsorbate separated from the relaxed water cluster and the total energy of the relaxed adsorbate-cluster system. The MPWB1K functional³⁸ and def2-TZVP basis set³⁹ were used in the implementation of Gaussian 09 (ref. 40) based on the benchmark performed by Lamberts and Kästner¹⁶. All density functional theory calculations comprise full geometry optimizations and all stationary points were verified by Hessian calculations; that is, by having zero imaginary frequencies.

In Supplementary Table 1, the structures of the adsorbate-cluster systems for the two water clusters and both adsorbates are displayed with their corresponding binding energies and zero-point energy corrections. The total binding energies are all of the same order of magnitude, ~ 10 kJ mol⁻¹; that is, ~ 0.1 eV. The interaction energy between a dimer of H₂S and H₂O is roughly 6 kJ mol⁻¹ (ref. 16). Note that the binding energy also contains a contribution related to the restructuring of the water cluster.

References

1. Williams, D. A. Physical adsorption processes on interstellar graphite grains. *Astrophys. J.* 151, 935–943 (1968).
2. Garrod, R. T., Wakelam, V. & Herbst, E. Non-thermal desorption from interstellar dust grains via exothermic surface reactions. *Astron. Astrophys.* 467, 1103–1115 (2007).
3. Vidal, T. H. G. et al. On the reservoir of sulphur in dark clouds: chemistry and

- elemental abundance reconciled. *Mon. Not. R. Astron. Soc.* 489, 435–447 (2017).
4. Dulieu, F. et al. How micron-sized dust particles determine the chemistry of our Universe. *Sci. Rep.* 3, 1338 (2013).
 5. Minissale, M., Dulieu, F., Cazaux, S. & Hocuk, S. Dust as interstellar catalyst. Quantifying the chemical desorption process. *Astron. Astrophys.* 585, A24 (2016).
 6. He, J., Emtiza, S. M. & Vidali, G. Mechanism of atomic hydrogen addition reactions on np-ASW. *Astrophys. J.* 851, 104 (2017).
 7. Tielens, A. G. G. M. The molecular universe. *Rev. Mod. Phys.* 85, 1021–1081 (2013).
 8. Hama, T. & Watanabe, N. Surface processes on interstellar amorphous solid water: adsorption, diffusion, tunneling reactions, and nuclear-spin conversion. *Chem. Rev.* 113, 8783–8839 (2013).
 9. van Dishoeck, E. F., Herbst, E. & Neufeld, D. A. Interstellar water chemistry: from laboratory to observations. *Chem. Rev.* 113, 9043–9085 (2013).
 10. Hama, T. et al. A desorption mechanism of water following vacuum- ultraviolet irradiation on amorphous solid water at 90 K. *J. Chem. Phys.* 132, 164508 (2010).
 11. Fayolle, E. C. et al. CO ice photodesorption: a wavelength-dependent study. *Astrophys. J. Lett.* 739, L36 (2011).
 12. Muñoz Caro, G. M. et al. New results on thermal and photodesorption of CO ice using the novel InterStellar Astrochemistry Chamber (ISAC). *Astron. Astrophys.* 522, A108 (2010).
 13. Cuppen, H. H. et al. Grain surface models and data for astrochemistry. *Space Sci. Rev.* 212, 1–58 (2017).
 14. Watanabe, N., Nagaoka, A., Shiraki, T. & Kouchi, A. Hydrogenation of CO on

- pure solid CO and CO–H₂O mixed ice. *Astrophys. J.* 616, 638–642 (2004).
15. Hidaka, H., Miyauchi, N., Kouchi, A. & Watanabe, N. Structural effects of ice grain surfaces on the hydrogenation of CO at low temperatures. *Chem. Phys. Lett.* 456, 36–40 (2008).
 16. Lamberts, T. & Kästner, J. Tunneling reaction kinetics for the hydrogen abstraction reaction $\text{H} + \text{H}_2\text{S} \rightarrow \text{H}_2 + \text{HS}$ in the interstellar medium. *J. Phys. Chem. A* 121, 9736–9741 (2017).
 17. Qi, J., Lu, D., Song, H., Li, J. & Yang, M. Quantum and quasiclassical dynamics of the multi-channel $\text{H} + \text{H}_2\text{S}$ reaction. *J. Chem. Phys.* 146, 124303 (2017).
 18. Fathe, K., Holt, J. S., Oxley, S. P. & Pursell, C. J. Infrared spectroscopy of solid hydrogen sulfide and deuterium sulfide. *J. Phys. Chem. A* 110, 10793–10798 (2006).
 19. Jiménez-Escobar, A. & Muñoz Caro, G. M. Sulfur depletion in dense clouds and circumstellar regions. I. H₂S ice abundance and UV-photochemical reactions in the H₂O-matrix. *Astron. Astrophys.* 536, A91 (2011).
 20. Collings, M. P. et al. A laboratory survey of the thermal desorption of astrophysically relevant molecules. *Mon. Not. R. Astron. Soc.* 354, 1133–1140 (2004).
 21. Watanabe, N. et al. Direct measurements of hydrogen atom diffusion and the spin temperature of nascent H₂ molecule on amorphous solid water. *Astrophys. J. Lett.* 714, L233–L237 (2010).
 22. van der Tak, F. F. S., Boonmanm, A. M. S., Braakman, R. & van Dishoeck, E. F. Sulphur chemistry in the envelopes of massive young stars. *Astron. Astrophys.* 412, 133–145 (2003).

23. Woods, P. M. et al. A new study of an old sink of sulphur in hot molecular cores: the sulphur residue. *Mon. Not. R. Astron. Soc.* 450, 1256–1267 (2015).
24. Taquet, V., Charnley, S. B. & Sipilä, O. Multilayer formation and evaporation of deuterated ices in prestellar and protostellar cores. *Astrophys. J.* 791, 1 (2014).
25. Calmonte, U. et al. Sulphur-bearing species in the coma of comet 67P/Churyumov–Gerasimenko. *Mon. Not. R. Astron. Soc.* 462, S253–S273 (2016).
26. Esplugues, G. B., Viti, S., Goicoechea, J. R. & Cernicharo, J. Modelling the sulphur chemistry evolution in Orion KL. *Astron. Astrophys.* 567, A95 (2014).
27. Holdship, J. et al. H₂S in the L1157-B1 bow shock. *Mon. Not. R. Astron. Soc.* 463, 802–810 (2016).
28. Cruz-Díaz, G. A., Muñoz Caro, G. M., Chen, Y.-J. & Yih, T.-S. Vacuum-UV spectroscopy of interstellar ice analogs I. Absorption cross-sections of polar-ice molecules. *Astron. Astrophys.* 562, A119 (2014).
29. Prasad, S. S. & Tarafdar, S. P. UV radiation field inside dense clouds: its possible existence and chemical implications. *Astrophys. J.* 267, 603–609 (1983).
30. Shen, C. J., Greenberg, J. M., Schutte, W. A. & van Dishoeck, E. F. Cosmic ray induced explosive chemical desorption in dense clouds. *Astron. Astrophys.* 415, 203–215 (2004).
31. Gerakines, P. A., Schutte, W. A., Greenberg, J. M. & van Dishoeck, E. F. The infrared band strengths of H₂O, CO and CO₂ in laboratory simulations of astrophysical ice mixtures. *Astron. Astrophys.* 296, 810–818 (1995).
32. Hama, T. et al. The mechanism of surface diffusion of H and D atoms on amorphous solid water: existence of various potential sites. *Astrophys. J.* 757, 185 (2012).

33. Miyauchi, N. et al. Formation of hydrogen peroxide and water from the reaction of cold hydrogen atoms with solid oxygen at 10 K. *Chem. Phys. Lett.* 456, 27–30 (2008).
34. Oba, Y., Osaka, K., Watanabe, N., Chigai, T. & Kouchi, A. Reaction kinetics and isotope effect of water formation by the surface reaction of solid H₂O₂ with H atoms at low temperatures. *Faraday Discuss.* 168, 185–204 (2014).
35. Minissale, M. & Dulieu, F. Influence of surface coverage on the chemical desorption process. *J. Chem. Phys.* 141, 014304 (2014).
36. Minissale, M., Moudens, A., Baouche, S., Chaabouni, H. & Dulieu, F. Hydrogenation of CO-bearing species on grains: unexpected chemical desorption of CO. *Mon. Not. R. Astron. Soc.* 458, 2953–2961 (2016).
37. Watanabe, N. & Kouchi, A. Ice surface reactions: a key to chemical evolution in space. *Prog. Surf. Sci.* 83, 439–489 (2008).
38. Zhao, Y. & Truhlar, D. G. Hybrid meta density functional theory methods for thermochemistry, thermochemical kinetics, and noncovalent interactions: the MPW1B95 and MPWB1K models and comparative assessments for hydrogen bonding and van der Waals interactions. *J. Chem. Phys. A* 108, 6908–6918 (2004).
39. Weigend, F., Häser, M., Patzelt, H. & Ahlrichs, R. RI-MP2: optimized auxiliary basis sets and demonstration of efficiency. *Chem. Phys. Lett.* 294, 143–152 (1998).
40. Frisch, M. J. et al. *Gaussian 09 Revision D.01* (Gaussian, Wallingford, CT, 2016).

Acknowledgements

The authors thank H. Hidaka, T. Hama and J. Kästner for discussions about chemical desorption. This work was partly supported by a Japan Society for the Promotion of

Science Grant-in-Aid for Specially Promoted Research (JP17H06087) and Grant-in-Aid for Young Scientists (A) (JP26707030). Computational resources were provided by the state of Baden-Württemberg through bwHPC and the German Research Foundation through grant number INST 40/467-1 FUGG.

Author contributions

Y.O. planned the experiments in consultation with N.W. and A.K. Y.O. and T.T. performed the experiments. T.L. performed the computational calculations on binding energy. All authors discussed the results. Y.O., T.L. and N.W. wrote the paper.

Additional information

Supplementary information accompanies this paper at <https://doi.org/10.1038/s41550-018-0380-9>.

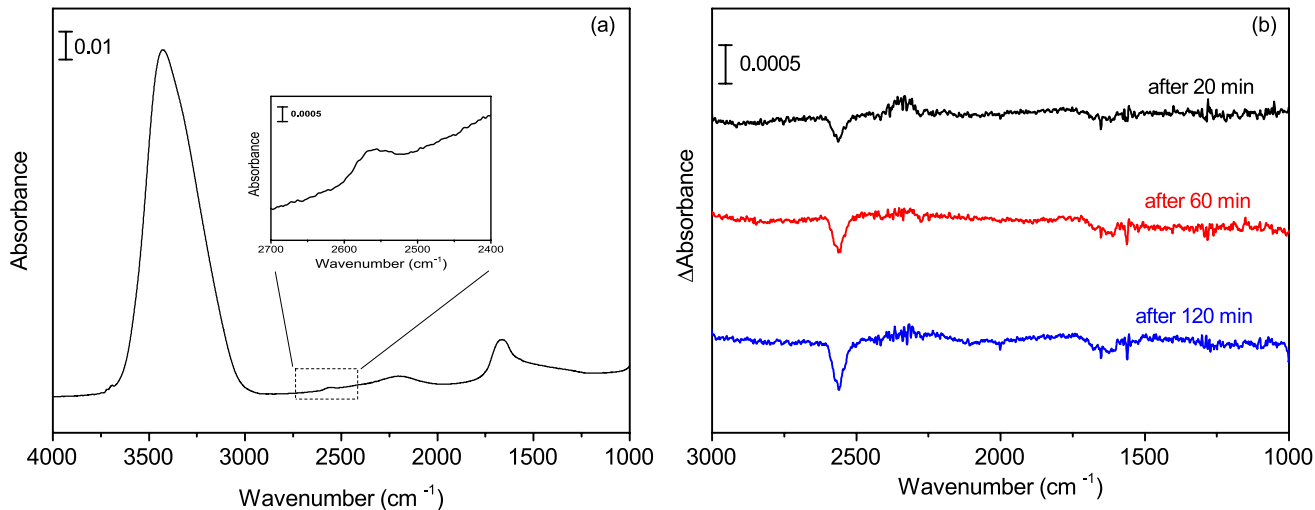


Fig. 1 FTIR spectra of samples. a. Solid H_2S (≈ 0.7 monolayer) deposited on ASW (~ 30 monolayers). The inset shows an enlarged spectrum focusing on the S-H stretching band of H_2S ($2,570\text{ cm}^{-1}$)¹⁸. Difference spectra after exposure to H atoms for 20 (top), 60 (middle) and 120 min (bottom). **b.** The spectral change at around $2,300\text{ cm}^{-1}$ is due to the temporal variation of atmospheric CO_2 concentration in the infrared beam line outside the vacuum chamber.

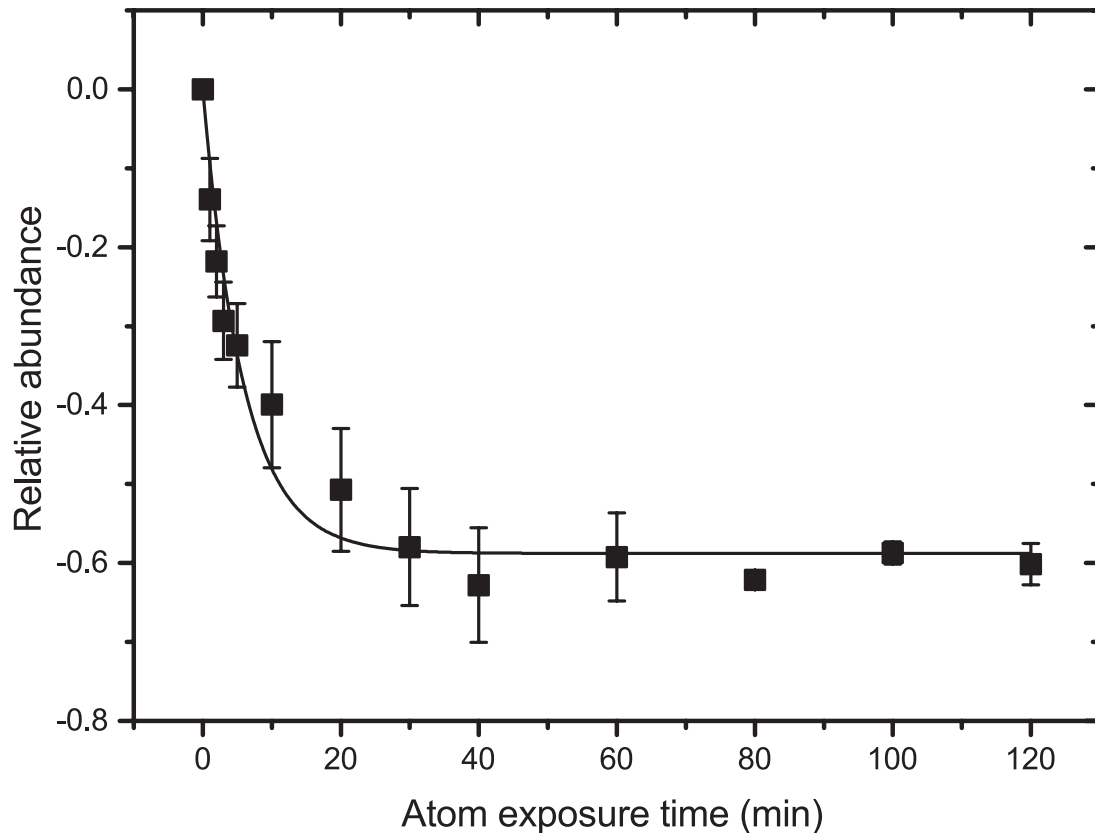


Fig. 2 Variations in the relative abundance of solid H_2S on ASW with relevance to H atom exposure times. The solid line is a single exponential fit to equation (1) (see MMethods). Each data point is an average of three measurements, with the s.d. of the mean values indicated by the error bars.

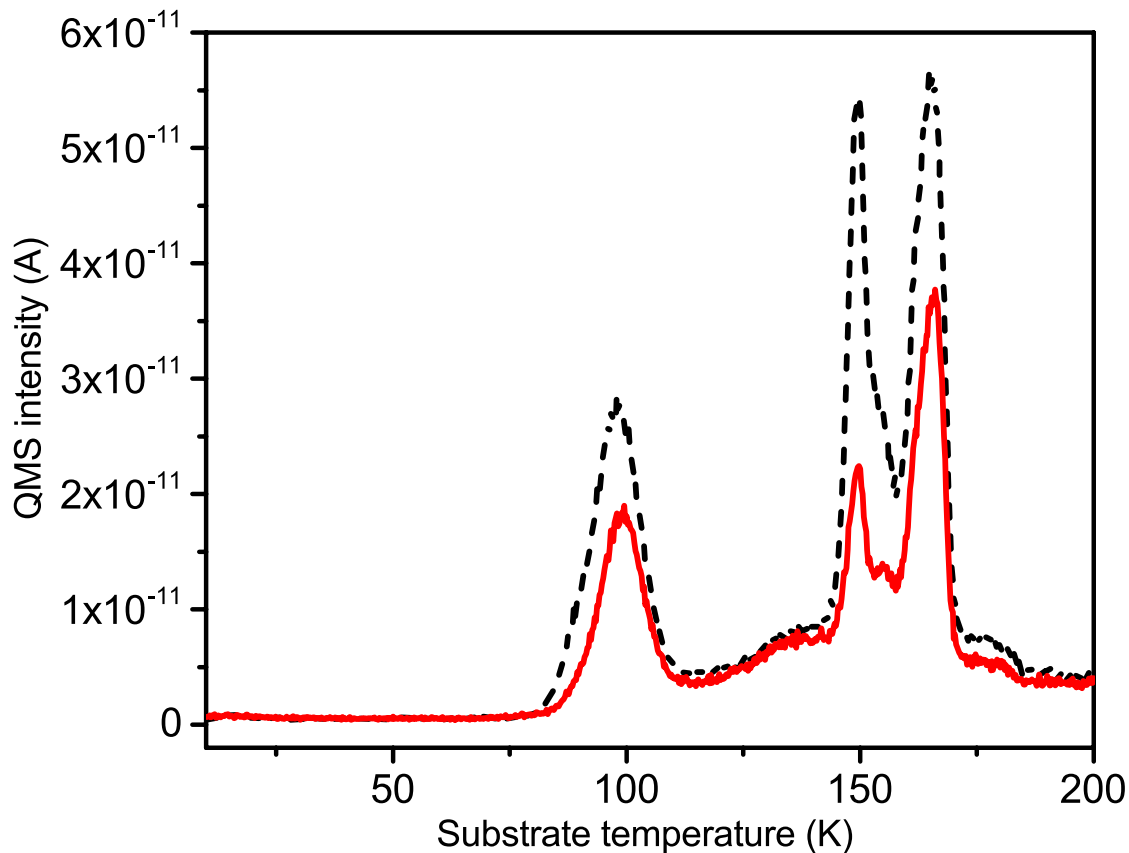


Fig. 3 TPD spectra. Solid H_2S ($m/z = 34$) from ASW obtained after exposure to H atoms (solid red line) and H_2 molecules without H atoms (H-blank experiment; dashed black line).

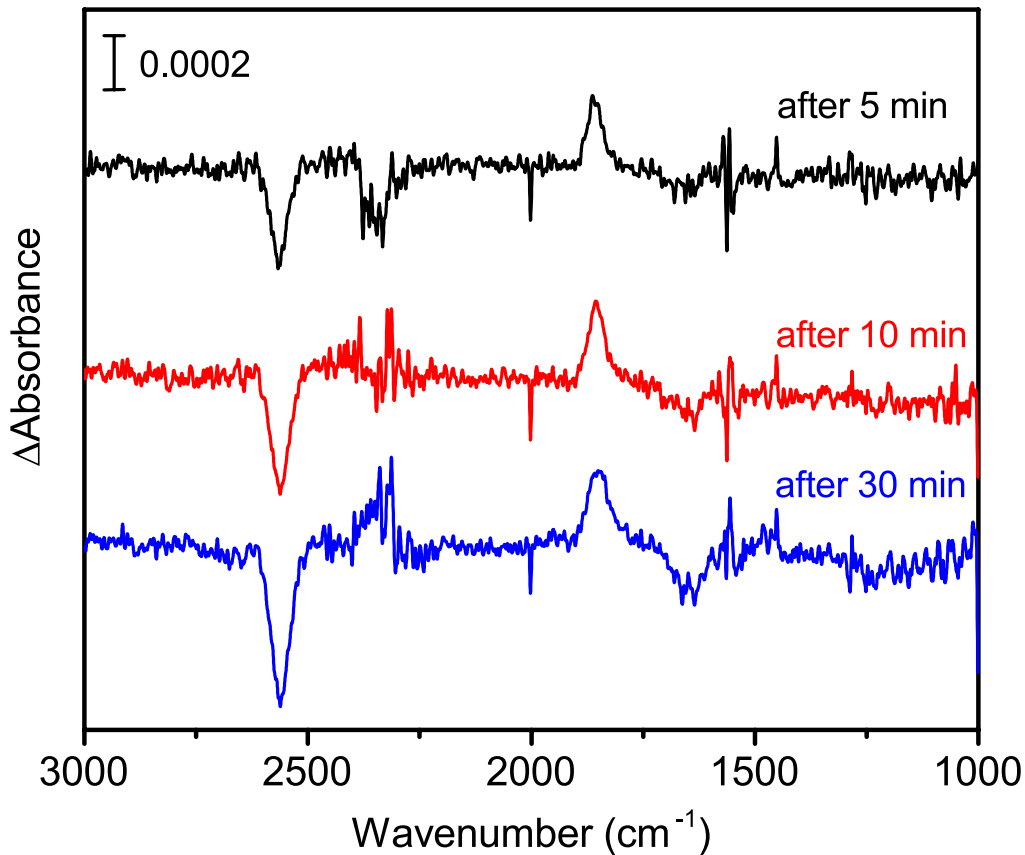


Fig. 4 Difference spectra of solid H₂S after exposure to D atoms for varying lengths of time on ASW. Top: 5 min. Middle: 10 min. Bottom: 30 min. The S-D stretching band of deuterated sulphides was observed at ~1,860 cm⁻¹. The spectral change at around 2,300 cm⁻¹ is due to the temporal variation of the atmospheric CO₂ concentration in the infrared beam line outside the vacuum chamber.